2009-07

High-spin structure of 37Cl, intruder excitations, and the sd-fp shell gap

Physical Review C,College Park,v. 80, n. 3, p. 034314-1-034314-12, Sept. 2009
http://www.producao.usp.br/handle/BDPI/49327

High-spin structure of ^{37}Cl, intruder excitations, and the *sd-fp* shell gap

M. Ionescu-Bujor,[1] A. Iordachescu,[1] S. M. Lenzi,[2] D. R. Napoli,[3] N. Mărginean,[1] N. H. Medina,[4] D. Bazzacco,[2] D. Bucurescu,[1] G. de Angelis,[3] F. Della Vedova,[2] E. Farnea,[2] A. Gadea,[3] R. Menegazzo,[2] S. Lunardi,[2] C. A. Ur,[1,2] S. Zilio,[2] T. Otsuka,[5,6] and Y. Utsuno[7]

[1]*National Institute for Physics and Nuclear Engineering, Bucharest, Romania*
[2]*Dipartimento di Fisica dell'Universitá and INFN, Sezione di Padova, Padova, Italy*
[3]*INFN, Laboratori Nazionali di Legnaro, Legnaro, Italy*
[4]*Instituto de Fisica, Universidade de São Paolo, São Paolo, Brazil*
[5]*University of Tokyo, Hongo, Tokyo 113-0033, Japan*
[6]*RIKEN, Hirosawa, Wako-shi, Saitama 351-0198, Japan*
[7]*Japan Atomic Energy Research Agency, Tokai, Ibaraki 319-1195, Japan*

(Received 11 May 2009; published 18 September 2009)

The structure of the $N = 20$ nucleus ^{37}Cl has been investigated in the ^{24}Mg(^{16}O,3p) reaction with a 70 MeV ^{16}O beam. A complex level scheme extended up to an excitation energy of 17 MeV and spins $(29/2^+)$ and $(27/2^-)$ on positive and negative parity, respectively, has been established. Lifetimes for the new states have been investigated by the Doppler shift attenuation method. Large-scale shell-model calculations have been performed in a valence space involving orbitals in the *sd* and *fp* shells using the *sdfp* and SDPF-M effective interactions. The comparison with the experimental data indicates the need for slight changes of the *sd-fp* energy gaps produced by these interactions.

DOI: 10.1103/PhysRevC.80.034314 PACS number(s): 27.30.+t, 21.60.Cs, 23.20.Gq, 23.20.Lv

I. INTRODUCTION

Considerable experimental and theoretical effort has been made in the last decade to elucidate the role of particle-hole *sd-fp* cross-shell intruder configurations in the structure of the *sd*-shell nuclei. At β stability, the experimental information, limited previously to low and medium spins [1], was extended to high spins and excitation energies, using heavy ion fusion-evaporation reactions and complex detection arrays [2–9]. In this region, the low-spin structure can be well reproduced by shell-model calculations limited to the *sd* main shell with the USD residual interaction introduced by Brown and Wildenthal [10]. At high spins, the excitations of particles from the *sd* shell to the *fp* shell have to be taken into account, and the experimental data serve as testing of the proposed effective interactions [11–14]. Interesting results pointing to a complex structure of coexisting spherical, deformed, and superdeformed states were recently reported in ^{36}Ar [2], ^{38}Ar [4], and ^{40}Ca [5], and described by large-scale shell-model calculations involving multiparticle-multihole intruder excitations from the *sd* to the *fp* shell [15].

The evolution of the nuclear structure in exotic neutron-rich *sd*-shell nuclei approaching the neutron $N = 20$ closure has attracted particular interest. The onset of deformation in the ground state of the neutron-rich $N = 20$ nuclei ^{32}Mg [16,17], ^{31}Na [18], and ^{30}Ne [19], referred to as the "island of inversion," is one of the most exciting features of the region. Particle-hole excitations of neutrons across the reduced $N = 20$ shell gap were found responsible for the observed features, as revealed by modern shell-model calculations including the *sd* and *fp* shells [12,20]. While the configuration of the ground state of nuclei in the island of inversion is dominated by *fp* intruder configurations, in heavier $N = 20$ nuclei, this configuration appears in excited states. The excitation energy of intruder states along the isotonic chain could provide useful information on the evolution of the *sd-fp* gap and on the residual interactions. In this respect, evidence for the presence of intruder configurations at low spin has been recently reported in ^{33}Al [21], ^{35}P [22], and ^{38}Ar [23].

The present work is focused on the $N = 20$ nucleus ^{37}Cl, with the aim of investigating the high-spin structure and identifying intruder configurations. Prior to our study, the information on high-spin states was very poor, especially for the positive parity, where the highest known spin was $7/2^+$ [1]. The experimental procedure and the new results obtained in spectroscopic studies and lifetime measurements are presented in Sec. II. A comparison of the experimental data with the predictions of large-scale shell-model calculations is given in Sec. III. The obtained results of the work are summarized in Sec. IV.

II. EXPERIMENTAL PROCEDURE AND RESULTS

The ^{37}Cl nucleus was populated via the ^{24}Mg(^{16}O,3p) reaction with a 70 MeV ^{16}O beam delivered by the XTU Tandem Accelerator of the Legnaro National Laboratory. Two independent experiments were performed. In the first experiment, devoted to the spectroscopic investigation, the target was a self-supporting ^{24}Mg foil with a thickness of 400 μg/cm^2. In the second experiment, a target consisting of 750 μg/cm^2 ^{24}Mg, backed with 15 mg/cm^2 ^{197}Au, was employed for lifetime determinations by the Doppler shift attenuation method (DSAM). Coincident γ rays were detected with the GASP array comprising 40 Compton-suppressed high-purity (HP) Ge detectors and an 80-element bismuth germanate (BGO) ball, which acts as a γ-ray multiplicity and sum-energy filter [24]. Events were collected when at

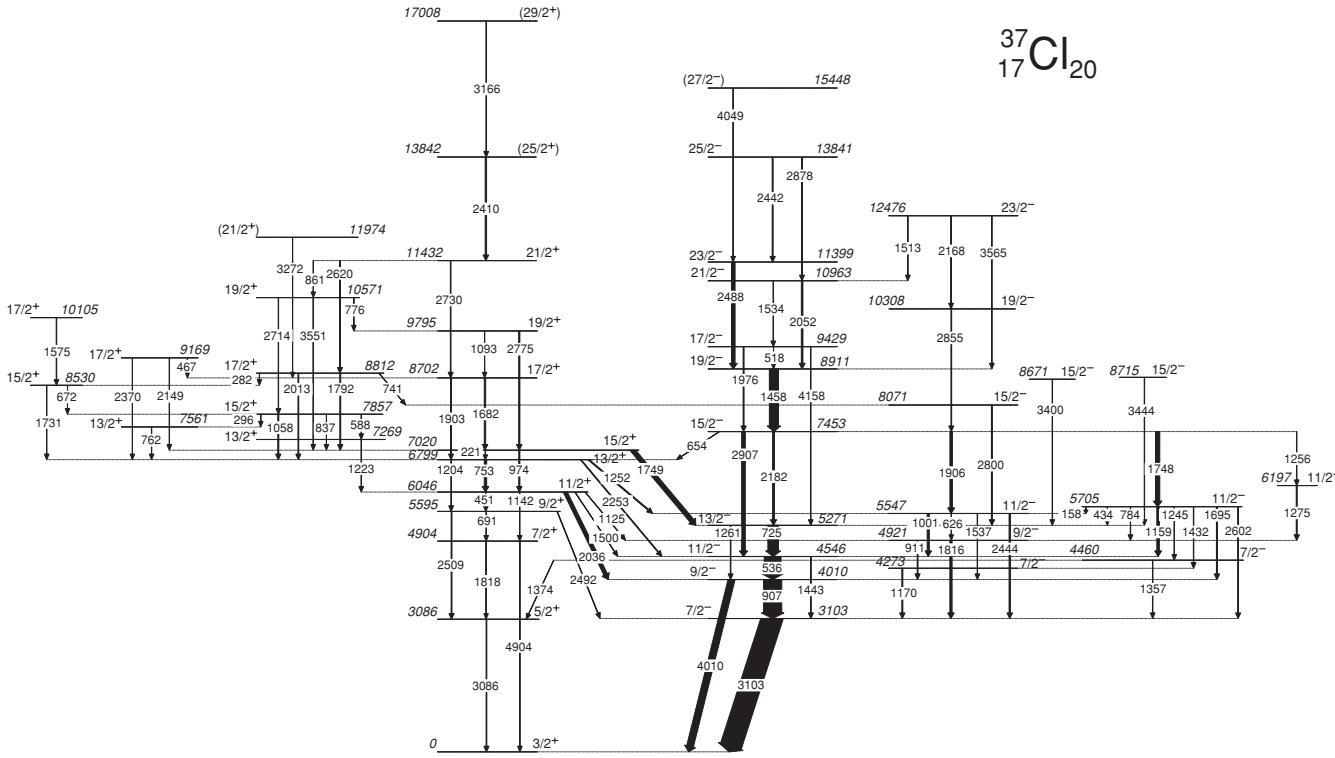

FIG. 1. Level scheme of ^{37}Cl established in the present experiment. The transitions between states of the same parity are shown as vertical arrows, while the transitions connecting states of different parities are shown as tilted arrows.

least two HPGe detectors and one BGO scintillator fired in coincidence. Energy and efficiency calibrations were performed with standard sources of ^{56}Co and ^{152}Eu. In the thin target experiment, for the purpose of channel selection and kinematical reconstruction, the Italian Silicon Sphere (ISIS) 4π charged-particle detector consisting of 40 ΔE-E Si telescopes [25] was also used.

The data from the thin target measurement have been sorted into several γ-γ matrices in coincidence with the detection of three protons. To improve the energy resolution, the kinematical reconstruction of the recoil direction has been performed. A symmetric γ-γ matrix and three asymmetric matrices having on the first axis the detectors in rings at 34°, 90°, and 146°, respectively, and on the second axis all the other detectors have been created. The symmetric matrix has been used to study γ-γ coincidence relationships for the construction of the level scheme, while the asymmetric matrices were used to obtain information about the γ transition multipolarities. For this purpose, the γ intensities corrected for efficiencies, from spectra gated on the axis with all the detectors, were used to calculate the ratio R_{ADO} defined as $R_{\mathrm{ADO}} = [I_\gamma(34°) + I_\gamma(146°)]/2I_\gamma(90°)$. In the present experimental conditions, the angular distribution ratios have the values $R_{\mathrm{ADO}} \approx 0.8$ for pure dipole stretched transitions ($I \to I - 1$), $R_{\mathrm{ADO}} \approx 1.35$ for quadrupole stretched transitions ($I \to I - 2$), and $R_{\mathrm{ADO}} \approx 1.4$ for transitions with $\Delta I = 0$. For transitions of $M1 + E2$ mixed character, R_{ADO} depends on the value and sign of the mixing coefficient δ, being $R_{\mathrm{ADO}} < 0.8$ for $\delta < 0$, and $R_{\mathrm{ADO}} > 0.8$ for $\delta > 0$.

The data registered in the gold-backed target experiment were sorted to create seven asymmetric γ-γ matrices having on the first axis the detectors in rings at 34°, 60°, 72°, 90°, 108°, 120° and 146°, respectively, and on the second axis all the other detectors. These matrices have been used for lifetime determinations.

A. Level scheme of ^{37}Cl

States in ^{37}Cl have been investigated previously by β and electron-capture (EC) decay, (p,γ), $(\alpha,p\gamma)$, transfer, and heavy-ion induced reactions [1]. The highest spins assigned in this nucleus were $I^\pi = 7/2^+$ and $I^\pi = 13/2^-$ for the 4904 and 5271 keV levels of positive and negative parity, respectively. In the present work, the level scheme was considerably extended at higher spins and excitation energies. A number of 28 new states have been observed and spin and parity was assigned to 34 levels: 18 of positive parity and 16 of negative parity. The deduced level scheme of the ^{37}Cl nucleus, containing 75 new γ transitions, is shown in Fig. 1. The energy and intensity of the observed transitions, the R_{ADO} ratios, and the assigned multipolarities, as well as the energy and spin assignments for the corresponding states, are given in Table I.

The level scheme has been constructed on the basis of coincidence relationships in background-corrected spectra created with appropriate gates on the symmetric γ-γ matrices from the thin target experiment. Illustrative background-subtracted coincidence spectra are shown in Figs. 2 and 3.

TABLE I. Transition energies, relative intensities of the γ rays, angular distribution ratios, multipolarities, initial state energies, and spin assignments for the initial and final states in ^{37}Cl.

E_γ (keV)	$I_\gamma^{\rm rel}$	$R_{\rm ADO}$	Mult.	E_x (keV)	I_i^π	I_f^π
157.6(3)	2(1)			5705	$11/2_3^-$	$11/2_2^-$
220.9(1)	12(1)			7020	$15/2_1^+$	$13/2_1^+$
281.6(3)	6(1)			8812	$17/2_2^+$	$15/2_3^+$
296.1(2)	2(1)			7857	$15/2_2^+$	$13/2_3^+$
434.4(1)	6(2)			5705	$11/2_3^-$	$13/2_1^-$
451.2(1)	27(2)	0.89(16)	$M1$	6046	$11/2_1^+$	$9/2_1^+$
467.3(9)	2(1)			9169	$17/2_3^+$	$17/2_1^-$
517.8(3)	5(2)			9429	$17/2_1^-$	$19/2_1^-$
535.7(1)	780(50)	0.84(2)	$M1$	4546	$11/2_1^-$	$9/2_1^-$
588.1(6)	4(2)			7857	$15/2_2^+$	$13/2_2^+$
626.4(2)	5(2)			5547	$11/2_2^-$	$9/2_2^-$
653.6(2)	11(3)	0.78(11)	$E1$	7453	$15/2_1^-$	$13/2_1^+$
671.6(2)	6(3)			8530	$15/2_3^+$	$15/2_2^+$
691.3(3)	8(2)	1.80(41)	$M1+E2$	5595	$9/2_1^+$	$7/2_1^+$
724.6(1)	374(30)	1.01(8)	$M1+E2$	5271	$13/2_1^-$	$11/2_1^-$
741.5(3)	5(2)	0.69(21)	$E1$	8812	$17/2_2^+$	$15/2_1^-$
753.4(1)	109(10)	0.87(11)	$M1$	6799	$13/2_1^+$	$11/2_1^+$
761.6(2)	13(3)	1.45(20)	$M1$	7561	$13/2_3^+$	$13/2_1^+$
776.1(9)	4(2)			10571	$19/2_2^+$	$19/2_1^+$
784.4(3)	14(2)	0.98(18)	$M1$	5705	$11/2_3^-$	$9/2_2^-$
837.4(3)	6(2)			7857	$15/2_2^+$	$15/2_1^+$
861.4(4)	5(2)			11432	$21/2_1^+$	$19/2_1^+$
906.8(1)	846(30)	1.45(8)	$M1+E2$	4010	$9/2_1^-$	$7/2_1^-$
911.2(5)	35(5)			4921	$9/2_2^-$	$9/2_1^-$
974.4(1)	50(9)	1.68(38)	$E2$	7020	$15/2_1^+$	$11/2_1^+$
1001.2(1)	96(10)	1.51(17)	$M1$	5547	$11/2_2^-$	$11/2_1^-$
1058.1(2)	45(5)	0.81(11)	$M1$	7857	$15/2_2^+$	$13/2_1^+$
1093.3(6)	4(2)			9795	$19/2_1^+$	$17/2_1^+$
1125.4(4)	14(4)	0.80(25)	$E1$	6046	$11/2_1^+$	$9/2_2^-$
1142.4(2)	11(3)	1.60(51)	$E2$	6046	$11/2_1^+$	$7/2_1^+$
1159.2(1)	116(4)	1.29(8)	$M1$	5705	$11/2_3^-$	$11/2_1^-$
1169.5(3)	44(5)	1.31(19)	$M1+E2$	4273	$7/2_2^-$	$7/2_1^-$
1204.4(2)	22(5)			6799	$13/2_1^+$	$9/2_1^+$
1222.7(4)	20(4)	0.75(12)	$M1$	7269	$13/2_2^+$	$11/2_1^+$
1244.6(6)	8(2)			5705	$11/2_3^-$	$7/2_3^-$
1252.4(3)	47(5)	0.83(10)	$E1$	6799	$13/2_1^+$	$11/2_2^-$
1256.4(3)	17(5)			7453	$15/2_1^-$	$11/2_4^-$
1260.6(1)	24(5)			5271	$13/2_1^-$	$9/2_1^-$
1275.4(3)	44(5)	0.85(11)	$M1$	6197	$11/2_4^-$	$9/2_2^-$
1357.1(3)	16(2)	1.26(22)		4460	$7/2_3^-$	$7/2_1^-$
1374.4(2)	11(2)			4460	$7/2_3^-$	$5/2_1^+$
1432.4(5)	18(2)			5705	$11/2_3^-$	$7/2_2^-$
1442.6(1)	34(4)	1.74(33)	$E2$	4546	$11/2_1^-$	$7/2_1^-$
1458.1(1)	422(29)	1.47(11)	$E2$	8911	$19/2_1^-$	$15/2_1^-$
1500.1(3)	15(4)	1.55(35)	$E1$	6046	$11/2_1^+$	$11/2_1^-$
1513.4(7)	24(3)	1.05(29)	$M1+E2$	12476	$23/2_2^-$	$21/2_1^-$
1534.2(3)	16(6)			10963	$21/2_1^-$	$17/2_1^-$
1537.2(2)	16(5)			5547	$11/2_2^-$	$9/2_1^-$
1574.6(3)	21(4)	0.85(21)	$M1$	10105	$17/2_4^+$	$15/2_3^+$
1681.6(2)	62(4)	1.37(19)	$M1+E2$	8702	$17/2_1^+$	$15/2_1^+$
1694.6(3)	45(3)	1.14(18)	$M1+E2$	5705	$11/2_3^-$	$9/2_1^-$
1730.6(1)	16(4)	0.82(22)	$M1$	8530	$15/2_3^+$	$13/2_1^+$
1747.6(1)	196(21)	1.65(20)	$E2$	7453	$15/2_1^-$	$11/2_3^-$
1749.4(1)	210(21)	0.80(13)	$E1$	7020	$15/2_1^+$	$13/2_1^-$
1791.6(3)	39(10)	0.51(14)	$M1+E2$	8812	$17/2_2^+$	$15/2_1^+$

TABLE I. (*Continued.*)

E_γ (keV)	$I_\gamma^{\rm rel}$	$R_{\rm ADO}$	Mult.	E_x (keV)	I_i^π	I_f^π
1816.6(3)	101(12)			4921	$9/2_2^-$	$7/2_1^-$
1818.1(4)	3(1)			4904	$7/2_1^+$	$5/2_1^+$
1903.2(5)	24(6)	1.50(38)	$E2$	8702	$17/2_1^+$	$13/2_1^+$
1906.0(1)	114(11)	1.51(17)	$E2$	7453	$15/2_1^-$	$11/2_2^-$
1975.6(3)	41(8)	0.59(12)	$M1+E2$	9429	$17/2_1^-$	$15/2_1^-$
2012.7(3)	33(3)	1.37(22)	$E2$	8812	$17/2_2^+$	$13/2_1^+$
2036.1(1)	172(12)	0.82(9)	$E1$	6046	$11/2_1^+$	$9/2_1^-$
2051.6(2)	71(7)	0.32(5)	$M1+E2$	10963	$21/2_1^-$	$19/2_1^-$
2148.7(12)	15(3)	0.77(25)	$M1$	9169	$17/2_3^+$	$15/2_1^-$
2168.4(14)	22(11)			12476	$23/2_2^-$	$19/2_2^-$
2181.6(1)	83(8)	0.52(6)	$M1+E2$	7453	$15/2_1^-$	$13/2_1^-$
2253.4(2)	33(5)	0.77(13)	$E1$	6799	$13/2_1^+$	$11/2_1^-$
2369.6(15)	7(2)			9169	$17/2_3^+$	$13/2_1^-$
2410.4(7)	61(7)	1.61(21)	$(E2)$	13842	$(25/2_1^+)$	$21/2_1^+$
2441.6(14)	40(9)			13841	$25/2_1^-$	$23/2_1^-$
2443.8(2)	60(11)			5547	$11/2_2^-$	$7/2_1^-$
2487.7(3)	158(33)	1.55(33)	$E2$	11399	$23/2_1^-$	$19/2_1^-$
2491.6(2)	22(2)			5595	$9/2_1^+$	$7/2_1^-$
2508.9(2)	36(3)			5595	$9/2_1^+$	$5/2_1^+$
2601.9(1)	35(4)			5705	$11/2_3^-$	$7/2_1^-$
2619.3(9)	31(5)	1.28(19)	$E2$	11432	$21/2_1^+$	$17/2_2^+$
2713.6(9)	16(7)			10571	$19/2_2^+$	$15/2_2^+$
2730.6(7)	29(8)	1.44(29)	$E2$	11432	$21/2_1^+$	$17/2_1^+$
2774.6(6)	52(5)	1.35(20)	$E2$	9795	$19/2_1^+$	$15/2_1^+$
2800.4(4)	44(5)	1.23(13)	$M1+E2$	8071	$15/2_2^-$	$13/2_1^-$
2855.3(14)	31(8)	1.57(41)	$E2$	10308	$19/2_2^-$	$15/2_1^-$
2878.3(8)	24(5)	1.52(33)	$E2$	13841	$25/2_1^-$	$21/2_1^-$
2906.8(1)	168(21)	1.42(19)	$E2$	7453	$15/2_1^-$	$11/2_1^-$
3086.2(5)	31(5)			3086	$5/2_1^+$	$3/2_1^+$
3103.2(1)	1000(19)	1.20(4)	$M2+E3$	3103	$7/2_1^-$	$3/2_1^+$
3165.6(9)	25(5)	1.38(24)	$(E2)$	17008	$(29/2_1^+)$	$(25/2_1^+)$
3271.8(13)	15(3)	1.22(24)	$(E2)$	11974	$(21/2_2^+)$	$17/2_1^+$
3399.6(11)	17(3)	0.83(16)	$M1$	8671	$15/2_3^-$	$13/2_1^-$
3444.3(15)	16(3)	0.75(16)	$M1$	8715	$15/2_4^-$	$13/2_1^-$
3551.5(17)	10(3)	1.25(38)	$E2$	10571	$19/2_2^+$	$15/2_1^+$
3564.6(14)	15(5)	1.5(6)	$E2$	12476	$23/2_2^-$	$19/2_1^-$
4009.6(1)	316(16)	1.43(9)	$E3$	4010	$9/2_1^-$	$3/2_1^+$
4048.6(25)	9(2)	1.6(4)	$(E2)$	15448	$(27/2_1^-)$	$23/2_1^-$
4158.4(13)	8(2)	1.5(4)	$E2$	9429	$17/2_1^-$	$13/2_1^-$
4903.7(23)	11(3)			4904	$7/2_1^+$	$3/2_1^+$

The spin assignments for the new levels were based on multipolarities of their deexciting transitions deduced from the $R_{\rm ADO}$ values. The general assumption of increasing spin at higher excitation energy has been applied. To increase the statistics and thus to reduce the error of the $R_{\rm ADO}$ ratio, for each analyzed transition, spectra were created using a sum of gates on transitions chosen carefully. $R_{\rm ADO}$ values lower than unity are providing an unambiguous indication on the dipole (eventually dipole+quadrupole) character of the $\Delta I = 1$ transitions, and therefore lead to firm spin assignments. On the other hand, $R_{\rm ADO}$ values around 1.4 indicate quadrupole stretched transitions, transitions with $\Delta I = 0$, as well as mixed $M1+E2$ transitions with a positive δ value. In the present study, many such transitions were observed (see Table I). For most cases, firm multipolarity and spin assignment was possible as the states of interest were fed and/or deexcited by more than one transition. For the highest excited states deexcited by only one transition, the assigned multipolarity and spin are tentative. All new stretched quadrupole transitions were assigned as $E2$. This assignment is supported by the lifetime measurements (see next section), as the $M2$ multipolarity would correspond to transition strengths much higher than the upper limit of 3 W.u. recommended for this mass region [26].

Some special features of the deduced level scheme are briefly discussed below. From a coincidence spectrum gated by the 4904 keV transition deexciting the $7/2^+$ state, several new transitions of relatively low energy (220, 451, 753, 691,

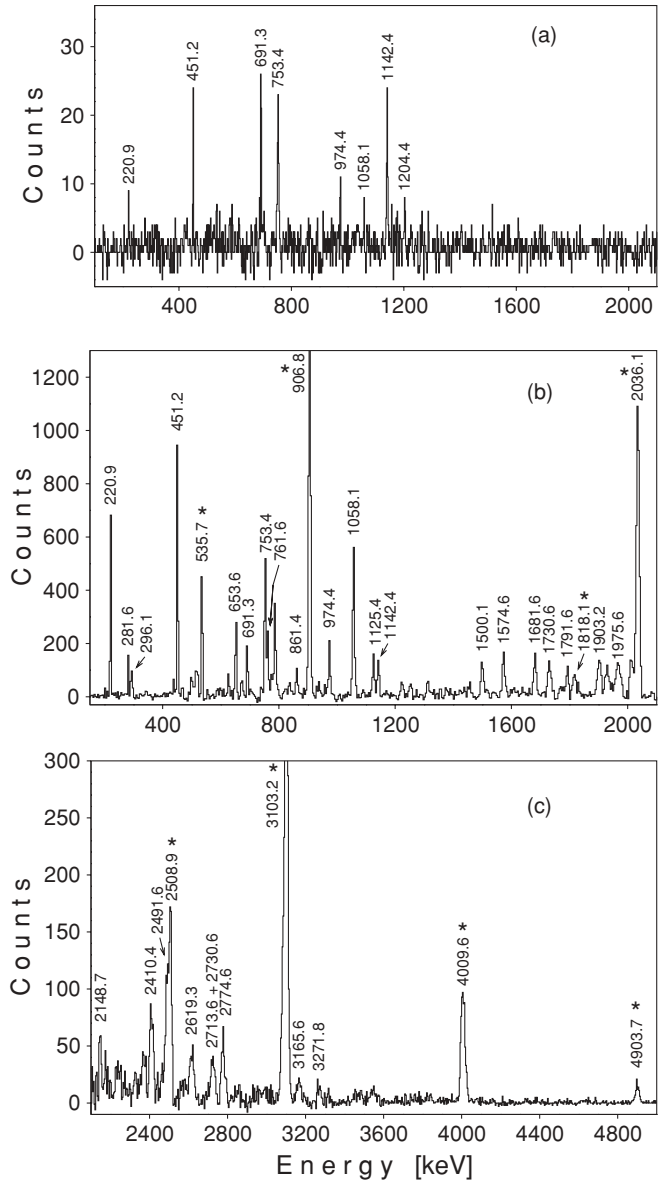

FIG. 2. Background-subtracted coincidence spectra obtained from the thin-target measurement: (a) gate on the 4904 keV γ ray; (b) and (c) gates on the 451, 753, and 974 keV γ rays. The γ rays in ^{37}Cl are labeled with the energy. The previously known γ rays are marked with a star.

974, 1142, and 1204 keV) have been observed [see spectrum of Fig. 2(a)]. They were included in a sequence of levels at 5595, 6046, 6799, and 7020 keV excitation energy, which were identified as the $9/2^+$, $11/2^+$, $13/2^+$, and $15/2^+$ yrast positive-parity states. The spin-parity assignment was based on the $M1$ and/or $E2$ character of the new transitions that are connecting these states between them and with the known $5/2^+$ and $7/2^+$ yrast states. Note that states at the energies of 5595, 6046, and 7020 keV were previously known in ^{37}Cl, but without spin-parity assignment [1]. The identified positive-parity states are linked to the negative-parity states by rather strong $E1$ transitions (see Fig. 1 and Table I), giving additional support to the spin assignment. The high-spin level scheme has been constructed on the basis of coincidence relationships in spectra created with appropriate gates, and the spin and parity was assigned based on the multipolarity given in Table I. Figures 2(b), 2(c), and 3 illustrate spectra in coincidence with the transitions in the low-lying positive- and negative-parity yrast sequences, respectively. The $15/2^-$ yrast state has been identified at 7453 keV; this state has a complex decay, feeding the $11/2^-$ and $13/2^-$ yrast states, as well as three yrare $11/2^-$ state. By a weak branch of 654 keV, it populates also the $13/2^+$ state. Two intense cascade quadrupole transitions of 1458 and 2488 keV feeding the 7453 keV state were assigned to deexcite the yrast $19/2^-$ and $23/2^-$ levels at 8911 and 11 399 keV, respectively. The yrast $17/2^-$ and $21/2^-$ states, identified at 9429 and 10 963 keV, are more weakly populated. Note the inversion observed in the yrast spin sequence, with the $19/2^-$ state below the $17/2^-$ state. The $17/2^+_1$ and $19/2^+_1$ states were identified at 8702 and 9795 keV, respectively, based on the observed $M1$ and $E2$ transitions linking them to the lower lying positive-parity yrast levels. The $21/2^+_1 \rightarrow 19/2^+_1$ and $23/2^-_1 \rightarrow 21/2^-_1$ transitions are missing, which indicates a different underlying structure. The $(25/2^+)$ and $25/2^-$ states have identical energy and similar populations. It was not possible to identify the $23/2^+$ and $27/2^+$ yrast states, suggesting their weak feeding. The level scheme was extended up to the spins $(29/2^+)$ and $(27/2^-)$ at excitation energy of 17 008 and 15 448 keV, respectively. Besides the yrast states, many yrare states have been also found, decaying mainly to the yrast states.

B. Lifetime measurements

In previous studies, lifetimes for the low-spin states in ^{37}Cl have been reported [1]. Lifetimes in the picosecond range, $T_{1/2}$ = 15(2), 23(2), 2.4(7), 2.4(6), and 2.1(11) ps, were measured for the 3103, 4010, 4546, 5271, and 7020 keV states, respectively. The other low-lying states have shorter lifetimes, in the femtosecond range.

In the present work, the lifetimes of the new high-spin states have been investigated by the Doppler shift attenuation method. The analysis has been performed using the LINESHAPE computer code [27], which incorporates MINUIT [28] for the error analysis. The slowing down history of ^{37}Cl recoils in the target and backing was simulated using Monte Carlo techniques, and a statistical distribution was created for the projection of the recoil velocity with respect to the direction of the detected γ ray. The code was modified to allow, at each level, side populations from independent levels. Moreover, the kinematic effects of the nucleon evaporation were included, as well as the finite solid angle of the detectors. The nuclear stopping power was taken from the theory of Lindhard, Scharff, and Schiøtt [29], using the approach in Ref. [30]. For the electronic stopping power, the Northcliffe-Schilling parametrization [31] corrected for atomic shell effects [32] was adopted. To estimate the systematic errors introduced by the adopted stopping powers, for several intense transitions the line-shape analysis has been also performed using the Ziegler stopping powers [33]. The lifetimes derived using the two parametrizations were found consistent within 5%. We assumed therefore a conservative uncertainty of 7% due to the stopping power.

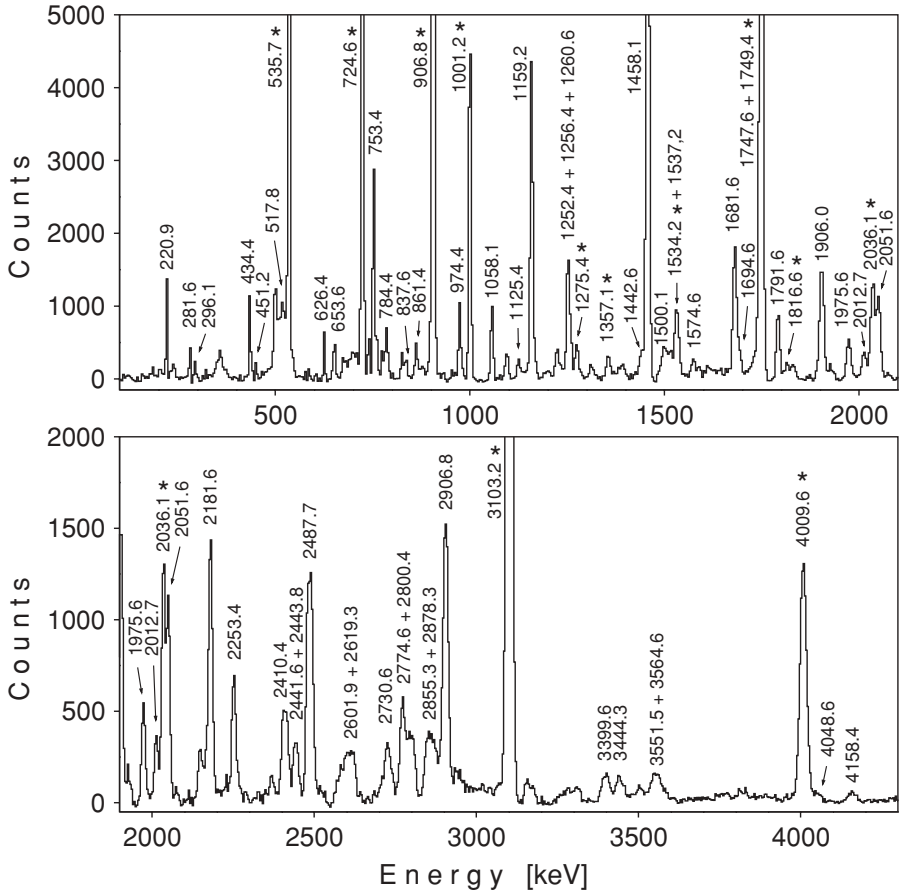

FIG. 3. Background-subtracted coincidence spectrum with gates on the transitions of 536, 725, 907, and 3103 keV from the thin-target measurement. The γ rays in ^{37}Cl are labeled with the energy. The previously known γ rays are marked with a star.

From the asymmetric γ-γ matrices obtained in the gold-backed target experiment, spectra have been created with narrow gates on the low-lying transitions of 3103, 907, and 535 keV, emitted from stopped nuclei. The line-shape analysis started with the transitions from the highest levels in ^{37}Cl and continued with the lower lying transitions. The obtained information for the higher levels was used in the analysis of the lower states. At each level, the intensity balance of feeding and decaying transitions was calculated using the γ intensities of Table I, allowing us to establish the amount of the fast side-feeding from unobserved transitions. Examples of experimental line shapes at different angles and the corresponding fits are illustrated in Fig. 4. The transitions of 3166, 2410, 2730, 2775, and 1682 keV on the positive-parity side and of 4049, 2442, 2488, and 2052 keV on the negative-parity side showed full Doppler shift in spectra registered at backward and forward detectors. An upper limit of about 0.1 ps was thus established for the lifetimes of yrast states with $I^\pi \geqslant 17/2^+$ and $I^\pi \geqslant 21/2^-$. The line-shape analysis for the intense 1458 keV transition (see Fig. 4) allowed us to derive the half-life $T_{1/2} = 0.69(8)$ ps for the $19/2^-$ 8911 keV yrast state. The $15/2^-_1$ 7453 keV state populated by the 1458 keV transition has also about 30% fast feeding. Its half-life was deduced as 0.13(4) ps from the analysis of the 1906 keV deexciting transition. Similarly, half-lives of 0.14(5) and 0.16(5) ps were derived for the $11/2^-_2$ 5547 keV and $11/2^-_3$ 5705 keV states, respectively, by analyzing the line shapes of the 1001 and 1160 keV transitions. The half-life $T_{1/2} = 2.4(6)$ ps previously assigned to the $13/2^-$ 5271 keV state [1] has been confirmed by the present measurement. As seen in Fig. 4, the shape of the 725 keV transition deexciting this state presents very small angle-dependent tails due to the rather long lifetime. On the positive-parity side, half-lives of 0.38(11), 0.85(15), and 0.41(7) ps were assigned to the $17/2^+_2$, $15/2^+_2$, and $13/2^+_1$ states, respectively. Figure 4 illustrates the line-shape analysis for the 753 keV transition deexciting the $13/2^+_1$ state at 6799 keV. The results of the present measurement concerning the lifetimes for seven new excited states in ^{37}Cl are collected in Table II.

III. DISCUSSION

To interpret the observed properties in ^{37}Cl, three shell-model calculations using different interactions and model spaces have been performed. A first calculation was performed with the code ANTOINE [34] in the *sd* shell-model space using the USD residual interaction [10]. The comparison between the experimental yrast positive-parity levels and the calculated ones is given in Table III. As seen in the table, agreement is obtained only for the first three lowest lying states, of spin $3/2^+$, $1/2^+$, and $5/2^+$. For $I^\pi \geqslant 7/2^+$, the calculated energies are much higher than experiment, which indicates that excitations to the *fp* shell might play an important role in the structure of these positive-parity states.

An exact diagonalization for ^{37}Cl was performed using the ANTOINE code in the $s_{1/2}d_{3/2}f_{7/2}p_{3/2}$ shell-model space. The

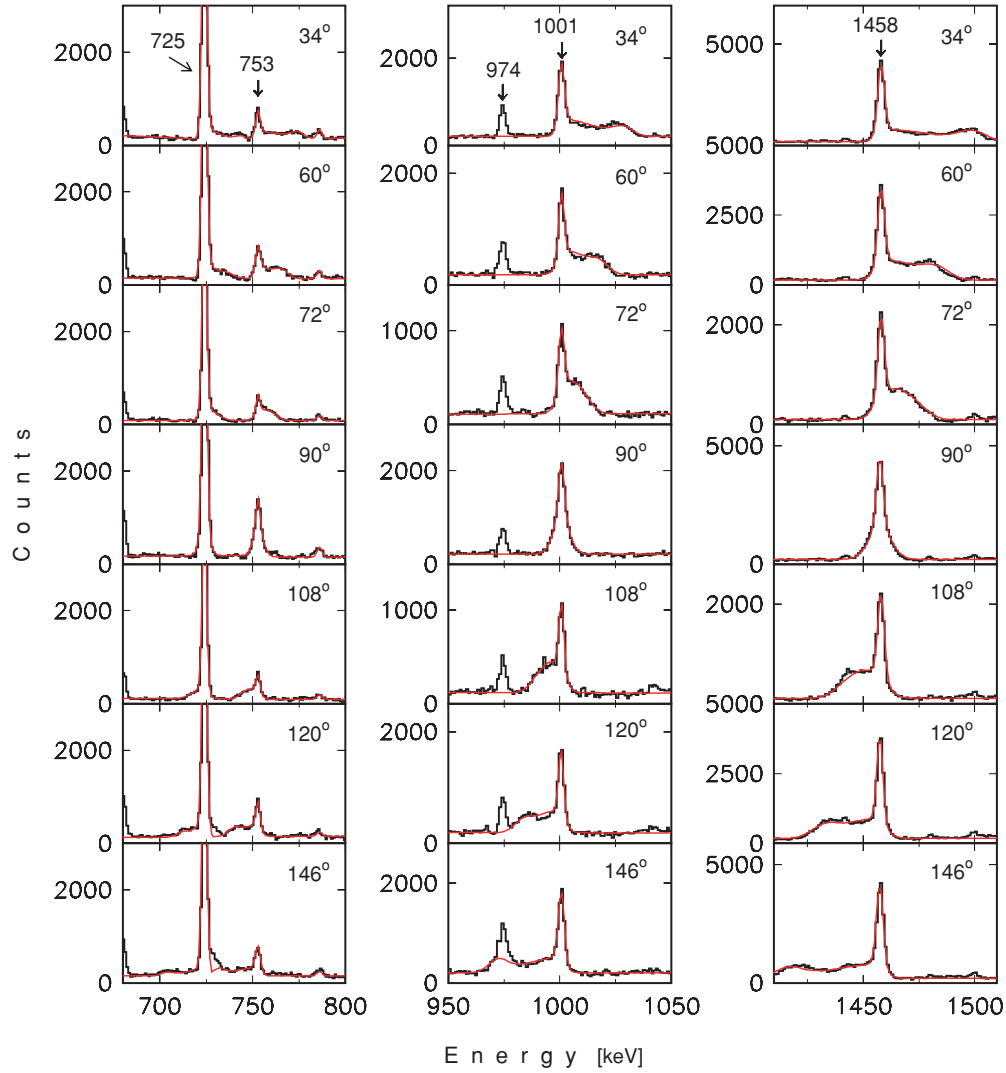

FIG. 4. (Color online) Experimental and calculated line shapes for the 725, 753, 1001, and 1458 keV transitions deexciting the states at 5271, 6799, 5547, and 8911 keV, respectively, in ^{37}Cl. The coincidence spectra were created with narrow gates on lower lying transitions emitted from stopped nuclei. For the 725 and 753 keV transitions, the analysis was performed using spectra gated by the 907 and 3103 keV transitions; while for the 1001 and 1458 keV transitions, a sum of spectra with gates on the 535, 907, and 3103 keV transitions, was used. The fitted DSAM spectra are shown in red.

truncated space assumes a ^{28}Si inert core, and therefore no excitations from the $d_{5/2}$ orbit are considered. The effective interaction, called *sdfp* [14], contains three parts: the USD interaction for the *sd*-shell [10], the KB' matrix elements for the *fp* shell [35], and the *G* matrix of Kahana, Lee, and Scott for the cross-shell matrix elements [36].

TABLE II. Half-lives determined in this work for new states in ^{37}Cl. The assigned errors include the uncertainties in the stopping power.

E_x (keV)	I^π	$T_{1/2}$ (ps)
5547	$11/2^-_2$	0.14(5)
5705	$11/2^-_3$	0.16(5)
6799	$13/2^+_1$	0.41(7)
7453	$15/2^-_1$	0.13(4)
7857	$15/2^+_2$	0.85(15)
8812	$17/2^+_2$	0.38(11)
8911	$19/2^-_1$	0.68(8)

TABLE III. Experimental yrast positive-parity states in ^{37}Cl (from Ref. [1] and present work) compared with calculations performed in the *sd* shell using the USD interaction [10].

I^π	$E_x^{\rm exp}$ (MeV)	$E_x^{\rm calc}$ (MeV)
$3/2^+$	0	0
$1/2^+$	1.726	1.838
$5/2^+$	3.087	3.265
$7/2^+$	4.904	7.645
$9/2^+$	5.595	7.671
$11/2^+$	6.046	14.763

The calculated level energies are compared with the experimental ones in Table IV and Fig. 5. The order of the yrast states is well reproduced, excepting the yrast $3/2^-$ state that is predicted below the yrast $5/2^-$ and $9/2^-$ states, in contrast to the experimental data.[1] In particular, the inversion observed at the spins $17/2^-$–$19/2^-$ is nicely confirmed by the calculation. The $23/2^+$ and $27/2^+$ states, not seen experimentally, are calculated at energies near the $25/2^+$ and $29/2^+$ yrast states, respectively, with the $23/2^+$ slightly above. This might correspond to lower populations for the $23/2^+$ and $27/2^+$ states, in accordance with the experimental findings.

While the overall features of the level scheme are well reproduced, the calculated energies are systematically smaller than the experimental ones. This is better illustrated in Fig. 6, which gives (in circle symbols) the differences between the energies derived in *sdfp* calculations and the experimental energies for yrast positive- and negative-parity states. As seen in the figure, these differences are rather small, around 0.3 MeV, only for the low-spin $1/2^+$ and $5/2^+$ states. At higher spin, the *sdfp* calculations underestimate the experimental energies, the difference increasing with spin. It is worth mentioning that detailed calculations using the same effective interaction have been recently reported for ^{36,38}Ar, and a similar underestimation of the experimental energies has been obtained (see Figs. 4 and 5 of Ref. [23]).

To have a deeper insight into the underlying structure, we have extracted the occupation numbers of protons and neutrons in the $f_{7/2}p_{3/2}$ orbits. The results are given in the Table IV. An interesting outcome of the calculations is the presence of intruder excitations in the structure of all levels in ^{37}Cl, the filling of the *fp* orbitals increasing with spin. Neutron excitations are more important than proton excitations. At low and medium spins of positive parity, two neutrons are promoted in the *fp* shell; while at spins equal to or larger than $21/2^+$, a neutron-proton pair is additionally promoted. Note that all the high-spin yrast states $\geqslant 15/2$ involve one proton promoted to the *fp* shell, except for the $19/2^+$ and $21/2^-$ yrast states, where the proton excitations are small. Because of this change in structure, the $21/2^+_1 \rightarrow 19/2^+_1$ and $23/2^-_1 \rightarrow 21/2^-_1$ transitions are strongly hindered, in nice agreement with the experimental decay pattern.

As the intruder excitations are present in the structure of all excited states in ^{37}Cl, the fact that the calculated energies are systematically smaller than the experimental energies could be an indication that the energy gap between the *sd* and *fp* shells has been somewhat underestimated in the *sdfp* calculations. New shell-model calculations have been therefore performed, increasing the $f_{7/2}$ and $p_{3/2}$ single-particle energies by 0.5 MeV. The results of these calculations, named $sdfp_1$, are shown in Table IV and Figs. 5 and 6. The modification of

[1]The level scheme for ^{37}Cl [1] contains a level at 3626.8 keV with $I^\pi = 3/2^{(+)}$ which was not included in the comparison with the calculations, as the assigned parity is only tentative. A negative parity is, however, not excluded, therefore this state could be the $3/2$ yrast negative-parity level. If this is so, the level ordering would be in accordance with the calculations.

TABLE IV. Experimental level energies in ^{37}Cl (from Ref. [1] and present work) compared with calculated values using the ANTOINE code in the $s_{1/2}d_{3/2}f_{7/2}p_{3/2}$ space and the *sdfp* and $sdfp_1$ interactions (details in text). Neutron (νfp) and proton (πfp) occupation numbers in the *fp* shell calculated with the *sdfp* interaction are given for each state.

I^π	$E_x^{\rm exp}$ (MeV)	$E_x^{\rm calc}$ (MeV)		νfp	πfp
		sdfp	$sdfp_1$		
$1/2^+$	1.73	1.43	1.48	1.66	0.38
	4.23	3.56	4.33	1.96	0.32
$3/2^+$	0	0	0	1.01	0.20
	3.71	3.03	3.60	2.20	0.25
$5/2^+$	3.09	2.84	3.27	2.07	0.25
	4.80	4.19	4.90	2.31	0.30
	5.49	4.28	5.21	1.95	0.25
$7/2^+$	4.90	3.74	4.76	2.34	0.21
$9/2^+$	5.59	4.49	5.53	2.28	0.24
$11/2^+$	6.05	4.87	5.91	2.29	0.28
$13/2^+$	6.80	5.42	6.42	2.19	0.41
	7.27	6.17	7.18	2.18	0.44
	7.56	6.35	7.47	1.89	0.82
$15/2^+$	7.02	5.73	6.78	2.23	0.36
	7.86	6.46	7.48	1.73	0.82
$17/2^+$	8.70	7.08	8.19	1.94	1.06
	8.81	7.83	8.83	2.27	0.48
	9.17	7.94	8.97	2.14	0.24
$19/2^+$	9.80	7.79	8.86	2.10	0.15
	10.57	9.10	10.24	2.22	1.02
$21/2^+$	11.43	9.31	11.05	2.90	1.08
	11.97	10.79	12.04	1.97	0.99
$23/2^+$		11.43	13.40	3.01	1.14
$25/2^+$	13.84	11.25	13.22	3.03	1.10
$27/2^+$		14.01	15.98	2.99	1.18
$29/2^+$	17.01	14.17	16.15	3.07	1.05
$3/2^-$	4.18	3.03	3.62	1.37	0.66
$5/2^-$	3.74	3.37	3.89	1.36	0.22
$7/2^-$	3.10	2.44	2.97	1.51	0.74
	4.27	3.56	4.36	1.97	0.59
	4.46	4.06	4.57	1.55	0.36
$9/2^-$	4.01	3.65	4.14	1.46	0.24
	4.92	4.34	4.85	1.53	0.36
	5.70	4.90	5.42	1.53	0.23
$11/2^-$	4.55	3.74	4.26	1.42	0.24
	5.55	4.58	5.22	2.40	0.80
	5.70	4.76	5.65	1.79	0.38
	6.20	5.47	6.22	1.75	0.49
$13/2^-$	5.27	4.29	4.80	1.45	0.15
$15/2^-$	7.45	6.41	7.91	2.59	1.01
	8.07	6.92	8.19	3.07	0.87
	8.67	7.52	8.60	2.57	0.55
$17/2^-$	9.43	8.06	9.59	2.63	0.82
$19/2^-$	8.91	7.61	9.13	2.36	1.09
	10.31	8.86	10.43	3.14	0.91
$21/2^-$	10.96	9.77	11.29	2.82	0.46
$23/2^-$	11.40	10.08	11.62	2.28	1.09
	12.48	10.66	12.18	2.34	1.10
$25/2^-$	13.84	12.99	14.48	2.17	1.08
$27/2^-$	15.45	13.46	14.99	2.18	1.06

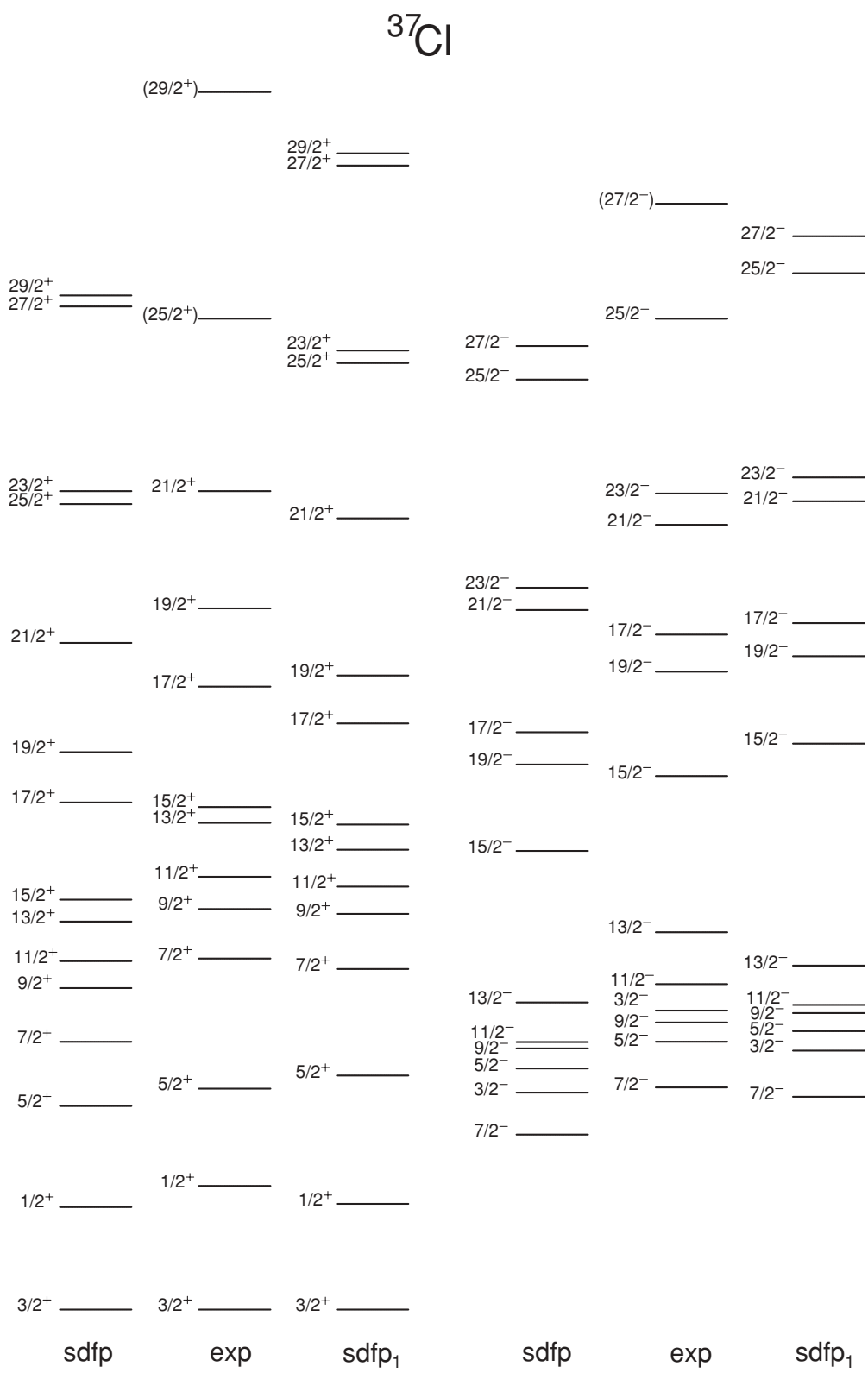

FIG. 5. Experimental yrast levels of ^{37}Cl compared to shell-model calculations using the ANTOINE code in the $s_{1/2}d_{3/2}f_{7/2}p_{3/2}$ space (see text for details).

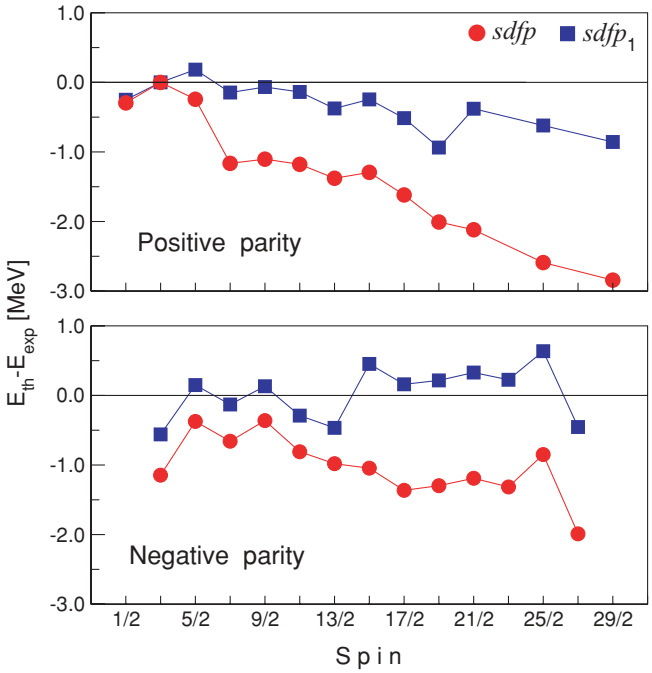

FIG. 6. (Color online) Difference between the shell-model calculated energies in the $s_{1/2}d_{3/2}f_{7/2}p_{3/2}$ space using the ANTOINE code and experimental energies for yrast states in ^{37}Cl (see text for details).

the energy gap has small influence on the wave functions. On the other hand, the calculated energies for all levels, both yrast and yrare, are in better agreement with the experimental data.

The *sdfp* effective interaction takes ^{28}Si as a core, and the single-particle energies are chosen in order to reproduce the single-particle states in ^{29}Si. The change in the gap between the *sd* and *fp* shells by 500 keV, which seems to give a better description of the spectroscopy of ^{37}Cl and other nuclei in this region such as ^{36}Ar and ^{38}Ar, does not reproduce well the ^{29}Si spectra. An alternative solution could be to change the matrix elements of the effective interaction that connect the *sd* with the *fp* shell, making them slightly more repulsive. This deserves a dedicated theoretical work that will benefit from detailed spectroscopy studies in this mass region.

The constraint of a closed ^{28}Si core has been released in a calculation done with the Monte Carlo shell model (MCSM) [37], using the SDPF-M interaction introduced in Refs. [12,13] and the $d_{5/2}s_{1/2}d_{3/2}f_{7/2}p_{3/2}$ valence space. The calculated level energies are compared with the experimental ones in Table V and Fig. 7. The contribution of nucleon excitation to the *fp* shell is rather small for the yrast $1/2^+$, $3/2^+$, and $5/2^+$ states, in accordance with the USD calculations (see Table III). In general the intruder contributions are smaller than those derived in the *sdfp* calculations. Similar to the *sdfp* calculations, the yrast $3/2^-$ state is predicted below the $5/2^-$ and $9/2^-$ yrast states. The experimental energies are rather well described by the MCSM calculations. An overestimation of about 400 keV is, however, observed for the calculated states, indicating that the $d_{3/2}$-$f_{7/2}$ gap produced by the SDFP-M interaction may be too large. It is worthwhile to mention that a similar conclusion was derived from recent MCSM calculations performed for ^{31}P [7].

TABLE V. Experimental level energies in ^{37}Cl (from Ref. [1] and present work) compared with MCSM calculations using the SDPF-M interaction. Neutron (νfp) and proton (πfp) calculated occupation numbers in the *fp* are given for each state.

I^π	$E_x^{\rm exp}$ (MeV)	$E_x^{\rm calc}$ (MeV)	νfp	πfp
$1/2^+$	1.73	1.84	0.53	0.24
	4.23	4.51	1.97	0.12
$3/2^+$	0	0.00	0.42	0.17
	3.71	3.72	2.03	0.10
$5/2^+$	3.09	3.47	0.61	0.17
	4.80	4.81	1.91	0.10
$7/2^+$	4.90	5.10	2.10	0.10
$9/2^+$	5.59	5.94	2.05	0.10
$3/2^-$	4.18	4.36	1.16	0.16
$5/2^-$	3.74	4.43	1.15	0.12
$7/2^-$	3.10	3.77	0.72	0.63
	4.27	5.05	0.98	0.30
$9/2^-$	4.01	4.78	1.17	0.14
	4.92	5.66	1.13	0.17
$11/2^-$	4.55	4.80	1.17	0.12
	5.55	6.09	1.16	0.14

Using the measured half-lives (from Ref. [1] and this work) and the branching ratios (BRs) derived from the presently determined γ-ray intensities, the experimental $B(M1)$ and $B(E2)$ reduced transition probabilities have been obtained.

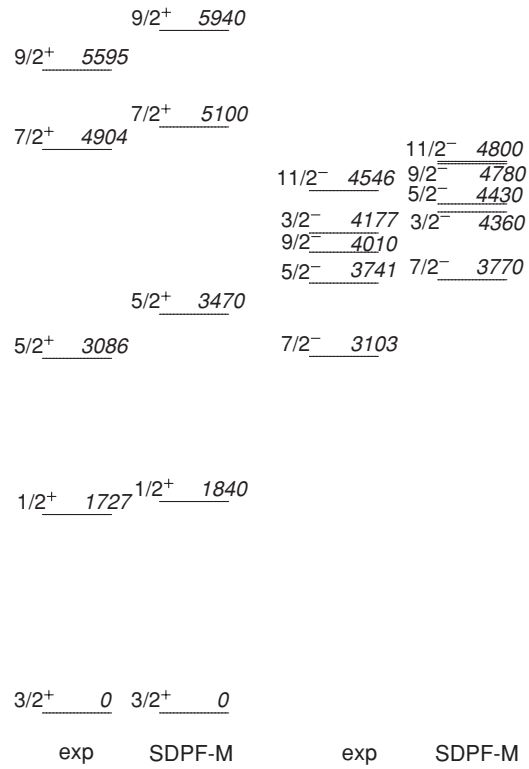

FIG. 7. Experimental yrast levels of ^{37}Cl compared to MCSM calculations with the SDPF-M interaction.

TABLE VI. Experimental reduced transition probabilities $B(M1)$ and $B(E2)$ in ^{37}Cl compared with shell-model calculations performed with the code ANTOINE in the $s_{1/2}d_{3/2}f_{7/2}p_{3/2}$ space using the *sdfp* and $sdfp_1$ residual interactions (see text for details). In deriving the theoretical $B(M1)$ values, free nucleon g factors have been used. The theoretical $B(E2)$ have been obtained using the effective electric charges of $e_\nu^{\rm eff} = 0.5e$ and $e_\pi^{\rm eff} = 1.5e$.

$E_{\rm lev}^{\rm exp}$ (keV)	$T_{1/2}^{\rm exp}$ (ps)	I^π	I_f^π	$E_\gamma^{\rm exp}$ (keV)	BR$_{\rm exp}$%	$B(M1)$ (μ_N^2)			$B(E2)$ (e^2 fm^4)		
						Exp	*sdfp*	$sdfp_1$	Exp	*sdfp*	$sdfp_1$
3086	0.027(6)[a]	$5/2_1^+$	$3/2_1^+$	3086	100	0.032(7)	0.029	0.037	26(7)	35	38
4904	0.024(11)[a]	$7/2_1^+$	$5/2_1^+$	1818	21(7)	0.056(3)	0.009	0.003			
			$3/2_1^+$	4904	79(8)				7(4)	5	3
6799	0.41(7)[b]	$13/2_1^+$	$11/2_1^+$	753	52(2)	0.117(29)	0.109	0.145			
			$9/2_1^+$	1204	10(2)				54(16)	37	36
7020	2.1(11)[a]	$15/2_1^+$	$13/2_1^+$	221	4(1)	0.070(39)	0.001	0.002			
			$11/2_1^+$	974	10(2)				55(32)	31	31
7857	0.85(15)[b]	$15/2_2^+$	$13/2_1^+$	1058	79(9)	0.031(8)	0.236	0.235			
8812	0.38(11)[b]	$17/2_2^+$	$15/2_1^+$	1792	47(9)	0.008(5)	0.039	0.038	3(2)	6	3
			$13/2_1^+$	2013	40(5)				18(7)	43	32
4273	0.075(30)[a]	$7/2_2^-$	$7/2_1^-$	1170	100	0.336(174)	1.069	1.183	12(6)	17	9
4460	0.055(20)[a]	$7/2_3^-$	$7/2_1^-$	1357	59(8)	0.164(66)	0.001	0.115			
4010	23(2)[a]	$9/2_1^-$	$7/2_1^-$	907	73(4)	0.0013(2)	0.036	0.049	6(1)	4	5
4921	0.055(30)[a]	$9/2_2^-$	$9/2_1^-$	911	26(6)	0.247(143)	0.000	0.008			
			$7/2_1^-$	1817	74(9)	0.089(50)	0.002	0.002			
4546	2.4(7)[a]	$11/2_1^-$	$9/2_1^-$	536	96(5)	0.103(60)	0.158	0.151			
			$7/2_1^-$	1443	4(1)				1.5(6)	0.0	0.4
5547	0.14(5)[b]	$11/2_2^-$	$11/2_1^-$	1001	54(3)	0.152(61)	0.099	0.001			
			$9/2_2^-$	626	3(1)	0.034(17)	0.073	0.071			
			$9/2_1^-$	1537	9(3)	0.007(3)	0.016	0.095			
			$7/2_1^-$	2444	34(8)				16(7)	48	21
5705	0.16(5)[b]	$11/2_3^-$	$11/2_2^-$	158	0.8(3)	0.506(295)	0.836	1.024			
			$11/2_1^-$	1159	48(2)	0.076(25)	0.071	0.074			
			$9/2_2^-$	784	6(2)	0.029(15)	0.064	0.652			
			$9/2_1^-$	1695	18(2)	0.009(4)	0.035	0.056	1.3(7)	1.4	1.2
			$7/2_3^-$	1245	3(1)				39(15)	1.8	2.6
			$7/2_2^-$	1432	7(10)				44(17)	36	6
			$7/2_1^-$	2602	14(2)				4(2)	0.4	9
5271	2.4(6)[a]	$13/2_1^-$	$11/2_1^-$	725	94(2)	0.040(12)	0.166	0.148	13(5)	16	17
			$9/2_1^-$	1261	6(2)				3(1)	10	11
7453	0.13(4)[b]	$15/2_1^-$	$13/2_1^-$	2182	12(2)	0.003(1)	0.000	0.001	0.4(2)	0.003	0.2
			$11/2_4^-$	1256	3(1)				42(15)	7	33
			$11/2_3^-$	1748	35(3)				92(33)	20	11
			$11/2_2^-$	1906	20(2)				35(11)	43	0.2
			$11/2_1^-$	2907	30(3)				6(2)	1	1
8911	0.68(8)[b]	$19/2_1^-$	$15/2_1^-$	1458	100				126(15)	52	67

[a]Ref. [1].
[b]Present study.

They are presented in Table VI together with the *sdfp* and $sdfp_1$ shell-model calculations. For $M1 + E2$ mixed transitions both $B(M1)$ and $B(E2)$ values have been deduced for comparison with shell-model calculations. In deriving the experimental values, the mixing coefficients δ from Ref. [1] have been used for the 3086, 1170, 907, and 725 keV transitions. For the newly identified transitions of 1792, 1695, and 2182 keV, values of, respectively, $\delta = -0.25(10)$, $+0.17(7)$, and $-0.20(7)$ deduced on the basis of $R_{\rm ADO}$ values from Table I were used. We note an overall agreement between experiment and calculations for the $B(E2)$ values. The $B(M1)$ values are nicely reproduced in many cases; however, for several states there are discrepancies. The $B(M1)$ reduced transition probabilities are more sensitive to the composition of the wave function, therefore the observed disagreement could be attributable to the truncated shell-model space, with the closed $d_{5/2}$ orbital.

IV. SUMMARY

The high-spin structure of the $N = 20$ nucleus ^{37}Cl has been investigated for the first time. The level scheme was extended up to an excitation energy of 17 MeV and spins

$(29/2^+)$ and $(27/2^-)$. Twenty-eight new levels have been observed. Lifetimes have been determined for seven new states by applying the Doppler shift attenuation method. The data were compared to large-scale shell-model calculations performed with the code ANTOINE using the *sdfp* effective interaction and to MCSM calculations with the SDPF-M interaction. The calculations have provided an overall good description of experimental data. Our study indicated that the shell gap between the *sd* and *fp* shells produced by the *sdfp* interaction is somewhat underestimated, while this is overestimated for SDPF-M interaction. Further investigations of the upper *sd*-shell nuclei would be helpful in pinning down the gap size more precisely and improving the interactions involving two main shells.

ACKNOWLEDGMENTS

This work was supported by the European Community FP6—Integrated Infrastructure Initiative—EURONS Contract No. RII3-CT-2004-506065. M.I-B., A.I., and N.M. acknowledge support from the Romanian National Authority for Scientific Research Contract IDEI 52/2007. N.H.M. acknowledges financial support from the Brazilian Agency CNPq and the Italian INFN.

[1] P. M. Endt, Nucl. Phys. **A633**, 1 (1998), and references therein.
[2] C. E. Svensson *et al.*, Phys. Rev. Lett. **85**, 2693 (2000).
[3] C. E. Svensson *et al.*, Phys. Rev. C **63**, 061301(R) (2001).
[4] D. Rudolph *et al.*, Phys. Rev. C **65**, 034305 (2002).
[5] E. Ideguchi *et al.*, Phys. Rev. Lett. **87**, 222501 (2001).
[6] P. Mason *et al.*, Phys. Rev. C **71**, 014316 (2005).
[7] M. Ionescu-Bujor *et al.*, Phys. Rev. C **73**, 024310 (2006).
[8] F. Della Vedova *et al.*, Phys. Rev. C **75**, 034317 (2007).
[9] R. Kshetri *et al.*, Nucl. Phys. **A781**, 277 (2007).
[10] B. A. Brown and B. H. Wildenthal, Annu. Rev. Nucl. Part. Sci. **38**, 29 (1988).
[11] E. K. Warburton, J. A. Becker, and B. A. Brown, Phys. Rev. C **41**, 1147 (1990).
[12] Y. Utsuno, T. Otsuka, T. Mizusaki, and M. Honma, Phys. Rev. C **60**, 054315 (1999).
[13] Y. Utsuno, T. Otsuka, T. Glasmacher, T. Mizusaki, and M. Honma, Phys. Rev. C **70**, 044307 (2004).
[14] E. Caurier, K. Langanke, G. Martinez-Pinedo, F. Nowacki, and P. Vogel, Phys. Lett. **B522**, 240 (2001).
[15] E. Caurier, F. Nowacki, and A. Poves, Phys. Rev. Lett. **95**, 042502 (2005).
[16] T. Motobayashi *et al.*, Phys. Lett. **B346**, 9 (1995).
[17] V. Tripathi *et al.*, Phys. Rev. C **77**, 034310 (2008).
[18] B. V. Pritychenko, T. Glasmacher, B. A. Brown, P. D. Cottle, R. W. Ibbotson, K. W. Kemper, L. A. Riley, and H. Scheit, Phys. Rev. C **63**, 011305(R) (2001).
[19] Y. Yanagisawa *et al.*, Phys. Lett. **B566**, 84 (2003).
[20] E. Caurier, F. Nowacki, and A. Poves, Nucl. Phys. **A693**, 374 (2001).
[21] V. Tripathi *et al.*, Phys. Rev. Lett. **101**, 142504 (2008).
[22] M. Wiedeking *et al.*, Phys. Rev. C **78**, 037302 (2008).
[23] A. F. Lisetskiy, E. Caurier, K. Langanke, G. Martínez-Pinedo, P. von Neumann-Cosel, F. Nowacki, and A. Richter, Nucl. Phys. **A789**, 114 (2007).
[24] C. Rossi Alvarez, Nucl. Phys. News **3**(3), 10 (1993).
[25] E. Farnea *et al.*, Nucl. Instrum. Methods Phys. Res. A **400**, 87 (1997).
[26] P. M. Endt, At. Data Nucl. Data Tables **23**, 3 (1979).
[27] J. C. Wells and N. R. Johnson, Report No. ORNL-6689, 1991, p. 44 (unpublished).
[28] F. James and M. Roos, Comput. Phys. Commun. **10**, 343 (1975).
[29] J. Lindhard, M. Scharff, and H. E. Schiøtt, K. Dan. Vidensk. Selsk. Mat.-Fys. Medd. **33**, No. 14 (1963).
[30] W. M. Currie, Nucl. Instrum. Methods **73**, 173 (1969).
[31] L. C. Northcliffe and R. F. Schilling, Nucl. Data Tables A **7**, 233 (1970).
[32] S. H. Sie, D. Ward, J. S. Geiger, R. L. Graham, and H. R. Andrews, Nucl. Phys. **A291**, 443 (1977).
[33] J. F. Ziegler, *The Stopping and Ranges of Ions in Matter*, Vols. 3 and 5 (Pergamon Press, New York, 1980).
[34] E. Caurier, Shell model code ANTOINE, Strasbourg, 1989–2004; E. Caurier and F. Nowacki, Acta Phys. Pol. **30**, 705 (1999).
[35] A. Poves and A. P. Zuker, Phys. Rep. **70**, 235 (1981).
[36] S. Kahana, H. C. Lee, and C. K. Scott, Phys. Rev. **180**, 956 (1969).
[37] T. Otsuka, M. Honma, and T. Mizusaki, Phys. Rev. Lett. **81**, 1588 (1998).